PAINLEVÉ'S PARADOX AND DYNAMIC JAMMING IN SIMPLE MODELS OF PASSIVE DYNAMIC WALKING

YIZHAR OR*

Abstract. Painlevé paradox occurs in rigid-body dynamics of mechanical systems with frictional contacts at configurations where the instantaneous solution is either indeterminate or inconsistent. Dynamic jamming is a scenario where the solution starts with consistent slippage and then converges in finite time to a configuration of inconsistency while the contact force grows unbounded. The goal of this paper is to demonstrate that these two phenomena are also relevant to the field of robotic walking, and can occur in two classical theoretical models of passive dynamic walking — the rimless wheel and the compass biped. These models typically assume sticking contact and ignore the possibility of foot slippage, an assumption which requires sufficiently large ground friction. Nevertheless, even for large friction, a perturbation that involves foot slippage can be kinematically enforced due to external forces, vibrations, or loose gravel on the surface. In this work, the rimless wheel and compass biped models are revisited, and it is shown that the periodic solutions under sticking contact can suffer from both Painlevé's paradox and dynamic jamming when given a perturbation of foot slippage. Thus, avoidance of these phenomena and analysis of orbital stability with respect to perturbations that include slippage are of crucial importance for robotic legged locomotion.

1. Introduction. Painlevé's paradox occurs in rigid-body mechanics of contact with dry friction, where the instantaneous solution of the contact dynamics becomes either inconsistent or indeterminate in certain configurations [27, 39]. This paradox has been demonstrated mathematically in simple models of a rigid rod or rectangular block sliding on a rough plane [23, 39] (Figure 1.1(a)), as well as more complicated models of multibody mechanisms with a single frictional contact [38]. In order to resolve Painlevé's paradox, one approach proposes regularization of the bodies' rigidity into an elastic contact interaction, followed by rigorous examination of the limit of infinite stiffness [21, 41, 44]. This approach works well for resolving cases of solution indeterminacy [35]. In configurations of inconsistency where no finite-force solution exists that satisfies the rigid-body assumptions along with Coulomb's friction law, it has been shown that there exists a consistent solution under *impulsive* contact forces [45], which is termed tangential impact [52], or impact without collision [4]. Although Painlevé's paradox and its resolution can be seen as a merely mathematical discussion stemming from the obvious shortcomings of rigid-body model and Coulomb's friction law, it appears that this paradox has roots in real-world physical phenomena of frictional contact dynamics. Examples are the "squeaking" caused by intermittent contact slippage of a chalk over a rough board [19], and the immediate bouncing out-of-contact of a robotic system on a frictional conveyor belt [55], which was inspired by the theoretical model studied in [23, 25]. Another phenomenon which is related to Painlevé's paradox is *dynamic jamming* [10, 38], where a rigid body or a multibody mechanism begins with consistent slippage and the dynamic solution reaches an inconsistent configuration in finite time, where the contact force grows unbounded. This scenario has been analyzed theoretically by Génot and Brogliato [14] for the rigid rod. Another mechanism of an inverted pendulum on a slider (IPOS) was proposed in [10, 38], see Figure 1.1(b), and its dynamic jamming solutions were analyzed. An early attempt to experimentally demonstrate dynamic jamming in an IPOS-like mechanism was made in [30], with only partial success. The main reason for the difficulties in experimental realization of Painlevé's paradox and dynamic jamming is

*Faculty of Mechanical Engineering, Technion - Israel Institute of Technology, Haifa 32000, Israel (izi@tx.technion.ac.il).

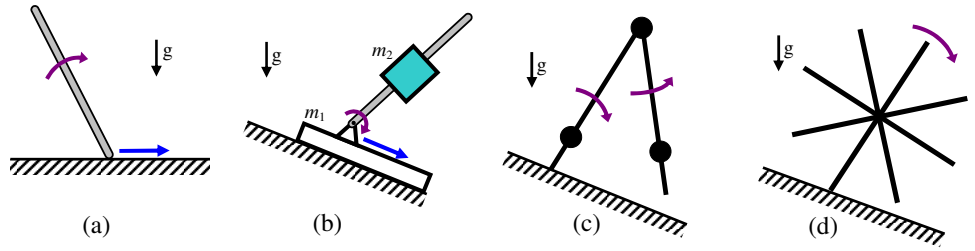

FIG. 1.1. *Examples of Painlevé's paradox and dynamic jamming – (a) The sliding rigid rod model. (b) Inverted pendulum on a slider (IPOS); Examples of passive dynamic walking – (c) The compass biped model. (d) The rimless wheel model.*

the fact that the conditions for their occurrence require extreme (and rare) values of physical parameters, and a narrow range of initial conditions. The goal of this paper is to demonstrate that Painlevé's paradox and dynamic jamming phenomena can also occur, at least theoretically, in another related and widely studied area — passive dynamic walking. The principle of passive dynamic walking has been exploited long time ago for bipedal toys walking down an inclined plane powered solely by gravity, without motors and actuation. The pioneering work of McGeer [28] was the first one to theoretically study passive dynamic walking and analyze orbital stability of its solutions. McGeer has studied a very simple model of a passive robotic walker what consists of two rigid links connected by a passive rotary joint (Figure 1.1(c)), which was later dubbed "compass biped" in [16]. He also identified in [28] that the passive dynamics of a biped is also very similar to the intermittent rolling motion of a rimless spoked wheel down an inclined plane, see Figure 1.1(d). Unlike the compass biped model, the low dimensionality of the rimless wheel model enables explicit analysis of its dynamics, as thoroughly studied by Coleman and Ruina in [6, 7]. Later on, the study of bipedal passive walking has been extended to account for knees [29], three-dimensional passive walker [9] and stabilization of lateral rocking [22]. More importantly, several works has studied these simple walking models with added actuation [49, 54]. It has been found that controlled actuation which is based on passive dynamics can significantly improve the energetic efficiency of powered walking [8]. In the last decade, feedback control of bipedal robotic walking has become a highly active research field, incorporating advanced techniques of nonlinear control [17, 20, 53]. Most of these works treat the robot's dynamics as a hybrid system [15], and orbital stability is analyzed by using the notion of Poincaré map [18] and its adaptation to hybrid systems [1, 32].

Importantly, almost all models of passive and actuated dynamic walking mentioned above make the key assumption that the foot that touches the ground (stance foot) makes a sticking contact without slippage, effectively resulting in a stationary pivot point on the ground. Additionally, these works assume inelastic impact in the collision of the free foot with the ground, which results in immediate sticking without slippage. These two assumptions implicitly require that the foot-ground friction is sufficiently large in order to prevent foot slippage. Only very few works analyzed the dynamics of bipedal walking under possible foot slippage [3, 48, 51], perhaps due to the added complexity of the dynamics. The recent work by Gamus and Or [11, 12] studies the dynamics of the two simple models of the rimless wheel and the compass biped in cases of insufficient ground friction that cannot maintain sticking contact of the stance foot at all times. Using numerical investigation, the onset of periodic so-

lutions with stick-slip transitions and/or slipping impacts is demonstrated in [11, 12], and their regions of existence and orbital stability are analyzed. In the case of actuated walking of the compass biped on a horizontal plane it is also shown in [11, 12] that a feedback law that indirectly enforces slippage at the foot impacts can significantly improve the energetic efficiency of walking, even for large friction under which a solution without slippage is also possible.

Another important observation is that even in cases where the ground friction is sufficiently large, foot slippage in legged robots can always be kinematically enforced at some instants, due to external disturbances and vibrations, non-ideal foot impacts, sudden motion of small loose objects on the terrain (e.g. gravel), as well as inaccuracies in the coordinated motion of the limbs in case of a multi-legged robot such as LittleDog [33] and BigDog [43]. Nevertheless, all works in the literature on dynamic legged locomotion study orbital stability only with respect to initial position-and-velocity perturbations that are restricted to satisfy the no-slip assumption. The dynamic response of a legged robot to a perturbation that enforces initial foot slippage is precisely the case where scenarios of Painlevé's paradox and dynamic jamming can occur. This may have a crucial influence on the robot's ability to overcome realistic perturbations and display practical stability with respect to slippage, which has not yet been studied.

This paper revisits the simplest two-dimensional models of passive dynamic walking — the rimless wheel and the compass biped, and studies the possible occurrence of Painlevé's paradox and dynamic jamming in classically stable periodic solutions. It is shown that the two key parameters that influence the likelihood of occurrence of Painlevé's paradox under small slippage perturbation along a periodic solution are large friction and small radius of gyration (i.e. most of the mass concentrated close to body's center). Using numerical simulation examples, it is shown that dynamic jamming can occur in the rimless wheel model only under a perturbation of large slippage along the periodic solution, and in the compass biped model only for initial conditions that lie away from the periodic solution. The paper is organized as follows. The next section gives a general formulation of the dynamics of a planar system with a single frictional contact, states the conditions for occurrence of Painlevé's paradox, and gives the definition of dynamic jamming. Sections 3 and 4, analyze the dynamics of the rimless wheel model and the compass biped model, respectively, under sticking contact as well as possible slippage, and study the occurrence of Painlevé paradox and dynamic jamming in these models. Finally, a concluding discussion is given in the closing section.

2. Problem Formulation. This section gives a systematic formulation of the dynamics of the rimless wheel and the compass biped models under possibility of either slippage or sticking contact. For greater generality, we consider a model of a planar biped robot that walk passively on a flat surface. The formulation is general enough to cover both the rimless wheel and the compass biped models, as well as other planar models with point feet. The robot can be either a single rigid body or a kinematic chain of rigid links, whose configuration is described by the coordinates $\mathbf{q} \in \mathbb{R}^N$. A particular material point on the robot, which is called the *stance foot*, is making contact with the ground. Another material point which is called *swing foot* is currently detached from the ground and is supposed to establish contact at the next step. When the swing foot hits the ground the stance foot is immediately detached, and the feet switch roles for the next step. The dynamics is composed of two phases — a continuous-time phase during which the swing foot moves forward,

and an instantaneous impact phase, caused by collision of the swing foot with the ground.

2.1. Continuous-time dynamics. Let $\mathbf{q} \in \mathbb{R}^N$ denote the coordinates which describe the position of each of the robot's links. In addition, the coordinates $\mathbf{q}$ also describe the position of the stance foot's contact point. Denoting $\mathbf{v}(\mathbf{q}, \dot{\mathbf{q}})$ as the velocity of the stance foot's endpoint, let v_t and v_n be the components of $\mathbf{v}(\mathbf{q}, \dot{\mathbf{q}})$ in the directions tangent and normal to the surface. These components can be formulated as

$$v_t = \mathbf{w}_t(\mathbf{q})^T \dot{\mathbf{q}} \ , \ v_n = \mathbf{w}_n(\mathbf{q})^T \dot{\mathbf{q}}. \tag{1}$$

When the foot makes a sticking contact with the ground, both v_t and v_n vanish, which gives the constraint in matrix form as

$$\mathbf{W}(\mathbf{q})\dot{\mathbf{q}} = 0, \text{ where } \mathbf{W}(\mathbf{q}) = \left[\mathbf{w}_t(\mathbf{q}) \ \ \mathbf{w}_n(\mathbf{q})\right]^T. \tag{2}$$

In case where the foot is slipping $v_t \neq 0$, only the constraint on the normal velocity $\mathbf{w}_n(\mathbf{q})^T \dot{\mathbf{q}} = 0$ holds.

The equations of motion of the robot can be formulated using the method of constrained Lagrange's equations (cf. [34]), as follows. Let $\mathcal{T}(\mathbf{q}, \dot{\mathbf{q}})$ be the total kinetic energy of the robot, and let $\mathcal{V}(\mathbf{q})$ be the robot's gravitational potential energy. The equations of motion are then given by

$$\mathbf{M}(\mathbf{q})\ddot{\mathbf{q}} + \mathbf{H}(\mathbf{q}, \dot{\mathbf{q}}) + \mathbf{G}(\mathbf{q}) = \mathbf{W}(\mathbf{q})^T \mathbf{f} \tag{3}$$

where

$$\mathbf{M}(\mathbf{q}) = \frac{\partial^2 \mathcal{T}}{\partial \dot{\mathbf{q}}^2}, \ \ \mathbf{H}(\mathbf{q}, \dot{\mathbf{q}}) = \left[\frac{\partial}{\partial \mathbf{q}}\left(\left(\frac{\partial \mathcal{T}}{\partial \dot{\mathbf{q}}}\right)^T\right)\right]\dot{\mathbf{q}} - \left(\frac{\partial \mathcal{T}}{\partial \mathbf{q}}\right)^T, \text{and } \mathbf{G}(\mathbf{q}) = \left(\frac{\partial \mathcal{V}}{\partial \mathbf{q}}\right)^T.$$

$\mathbf{M}(\mathbf{q})$ is called the matrix of inertia, $\mathbf{H}(\mathbf{q}, \dot{\mathbf{q}})$ is the vector of velocity-dependent terms such as Coriolis and centripetal forces, and the vector $\mathbf{G}(\mathbf{q})$ is the gravitational forces. On the right hand side of (3), the vector $\mathbf{f} = [f_t \ \ f_n]^T$ is the normal and tangential components of the contact force acting at the stance foot. Note that $\mathbf{W}(\mathbf{q})$ in (2) and (3) can be interpreted as the robot's Jacobian with respect to the stance foot's position, and that $\mathbf{f}$ can be regarded as the vector of Lagrange multipliers which give the magnitude of constraint forces, cf. [34]. When the foot is in sticking contact, the robot's motion is governed by (3) while the constraint (2) is satisfied. In order to compute the contact force $\mathbf{f}$, one has to differentiate the constraint (2) with respect to time and then substitute the expression for the accelerations $\ddot{\mathbf{q}}$ from (3), which gives

$$0 = \mathbf{W}\ddot{\mathbf{q}} + \dot{\mathbf{W}}\dot{\mathbf{q}} = \mathbf{W}\mathbf{M}^{-1}(-\mathbf{H} - \mathbf{G} + \mathbf{W}^T\mathbf{f}) + \dot{\mathbf{W}}\dot{\mathbf{q}}, \tag{4}$$

where the dependence in $\mathbf{q}$ and $\dot{\mathbf{q}}$ is suppressed for brevity. From (4), the contact force $\mathbf{f}$ is obtained as

$$\mathbf{f}_{stick}(\mathbf{q}, \dot{\mathbf{q}}) = \left(\mathbf{W}\mathbf{M}^{-1}\mathbf{W}^T\right)^{-1}\left(\mathbf{W}\mathbf{M}^{-1}(\mathbf{H} + \mathbf{G}) - \dot{\mathbf{W}}\dot{\mathbf{q}}\right). \tag{5}$$

Importantly, contact sticking can be maintained only if the friction between the foot and the ground is sufficiently large. Using Coulomb's dry friction model, this implies

that the tangential and normal components of the contact force $\mathbf{f}$ obtained in (5) must satisfy the inequality given by

$$|f_t| \leq \mu f_n, \tag{6}$$

where $\mu \geq 0$ is the coefficient of friction, which is assumed to be a given property of the contacting surfaces. When inequality (6) is not satisfied, tangential slippage of the contact point starts to evolve, i.e. $v_t \neq 0$. In that case, according to Coulomb's friction model, the tangential contact force f_t opposes the direction of slippage, and depends on the normal force f_n as $f_t = -\mathrm{sgn}(v_t)\mu f_n$. (For simplicity, we do not distinguish between static and kinetic friction throughout this work). This can also be written in matrix form as

$$\mathbf{f} = \mathbf{\Gamma} f_n, \text{ where } \mathbf{\Gamma} = \begin{pmatrix} 1 \\ -\mathrm{sgn}(v_t)\mu \end{pmatrix}. \tag{7}$$

The contact force $\mathbf{f}$ under slippage cannot be computed as in (5), since the constraint (2) is not satisfied. Instead, one has to differentiate the normal velocity constraint $\mathbf{w}_n(\mathbf{q})^T\dot{\mathbf{q}} = 0$ with respect to time and substitute the expression for $\ddot{\mathbf{q}}$ from (3) in order to obtain

$$0 = \mathbf{w}_n^T\ddot{\mathbf{q}} + \dot{\mathbf{w}}_n\dot{\mathbf{q}} = \mathbf{w}_n^T\mathbf{M}^{-1}(-\mathbf{H} - \mathbf{G} + \mathbf{W}^T\mathbf{\Gamma} f_n) + \dot{\mathbf{w}}_n\dot{\mathbf{q}}. \tag{8}$$

From (8), the normal force f_n can be obtained. Using (7), the contact force $\mathbf{f}$ is then given by

$$\mathbf{f}_{slip}(\mathbf{q}, \dot{\mathbf{q}}) = \mathbf{\Gamma}\left(\mathbf{w}_n^T\mathbf{M}^{-1}\mathbf{W}^T\mathbf{\Gamma}\right)^{-1}\left(\mathbf{w}_n^T\mathbf{M}^{-1}(\mathbf{H} + \mathbf{G}) - \dot{\mathbf{w}}_n\dot{\mathbf{q}}\right). \tag{9}$$

Contact slippage is maintained as long as $v_t = \mathbf{w}_t(\mathbf{q})\dot{\mathbf{q}} \neq 0$. When v_t vanishes, a transition to sticking contact occurs if the contact force $\mathbf{f}$ in (5) satisfies (6). Otherwise, slip reversal occurs and v_t reverses its sign.

2.2. Impact law. We now formulate the impact interaction that occurs when the swing foot collides with the ground. This part is given here for completeness of the model, but is is not necessary for analysis of Painlevé's paradox, which occurs at the continuous-time phase. Thus, the glancing reader may skip to part 2.3 at this point. The assumption of perfectly rigid bodies implies that a collision results in an instantaneous change in the velocities which is caused by impulsive contact forces. In this way, analysis of the very short time of complex contact interaction that involves local deformations is circumvented. In almost all the works on dynamic legged locomotion with point feet, it is assumed that the collision is governed by impulsive force acting at the colliding foot only. Furthermore, a perfectly plastic collision is assumed, which results in complete sticking of the colliding foot right after the impact, i.e. no (normal) rebound and no (tangential) slippage. We adopt the same simplifying assumptions in this work, with a natural extension to nonzero slippage in case where the perfectly plastic contact impulse does not satisfy the friction bounds.

Let $\tilde{\mathbf{v}}$ denote the velocity of the swing foot's endpoint during motion, where its tangential and normal components $\tilde{v}_t$, $\tilde{v}_n$ depend on $\mathbf{q}$ and $\dot{\mathbf{q}}$ according to

$$\tilde{\mathbf{v}} = \begin{pmatrix} \tilde{v}_t \\ \tilde{v}_n \end{pmatrix} = \begin{pmatrix} \tilde{\mathbf{w}}_t(\mathbf{q})^T \\ \tilde{\mathbf{w}}_n(\mathbf{q})^T \end{pmatrix}\dot{\mathbf{q}} = \tilde{\mathbf{W}}(\mathbf{q})\dot{\mathbf{q}}. \tag{10}$$

At the time t=t_c, the swing foot hits the ground, and an impact occurs. An impulsive contact force $\tilde{\mathbf{F}}$ acts instantaneously at the collision point. (The impulse $\tilde{\mathbf{F}}$ is the time-integral of the contact force $\tilde{\mathbf{f}}$ during the short period of contact, i.e. $\tilde{\mathbf{F}} = \int \tilde{\mathbf{f}}(t)dt$). It is assumed that the coordinates $\mathbf{q}$ remain unchanged during the collision $\mathbf{q}(t = t_c) = \mathbf{q}_c$, and that the velocities $\dot{\mathbf{q}}$ change instantaneously according to the impulse-momentum balance given by

$$\Delta\dot{\mathbf{q}} = \dot{\mathbf{q}}(t_c^+) - \dot{\mathbf{q}}(t_c^-) = \mathbf{M}_c^{-1}\tilde{\mathbf{W}}_c^T\tilde{\mathbf{F}}, \tag{11}$$

where the superscripts '+' and '−' denote the times right after and right before the collision, and $\mathbf{M}_c$ and $\mathbf{W}_c$ are shorthand notations to $\mathbf{M}(\mathbf{q} = \mathbf{q}_c)$ and $\mathbf{W}(\mathbf{q} = \mathbf{q}_c)$, respectively. (The relation (11) can be obtained from time-integration of equation (3) during the short collision where $\mathbf{W}(\mathbf{q})^T\mathbf{f}$ is replaced with $\tilde{\mathbf{W}}(\mathbf{q})^T\tilde{\mathbf{f}}$, while the contribution of $\mathbf{H}$, $\mathbf{G}$ and $\mathbf{f}$ is assumed negligible compared to that of $\tilde{\mathbf{f}}$.)

Assuming a perfectly plastic collision, the impact results in sticking contact at the colliding foot, i.e. $\tilde{\mathbf{v}}(t_c^+) = 0$. Using relations (10) and (11), one obtains

$$\tilde{\mathbf{W}}_c\dot{\mathbf{q}}_c^+ = \tilde{\mathbf{W}}_c(\dot{\mathbf{q}}_c^- + \mathbf{M}_c^{-1}\tilde{\mathbf{W}}_c^T\tilde{\mathbf{F}}) = 0 \tag{12}$$

where $\dot{\mathbf{q}}_c^+$ and $\dot{\mathbf{q}}_c^-$ are shorthand notations to $\dot{\mathbf{q}}(t = t_c^+)$ and $\dot{\mathbf{q}}(t = t_c^-)$, respectively. From (12), the contact impulse $\tilde{\mathbf{F}}$ can be obtained as

$$\tilde{\mathbf{F}}_{stick} = -\left(\tilde{\mathbf{W}}_c\mathbf{M}_c^{-1}\tilde{\mathbf{W}}_c^T\right)^{-1}\tilde{\mathbf{W}}_c\dot{\mathbf{q}}_c^-. \tag{13}$$

Substituting (13) into (11) then gives a linear relation between the pre-impact and post-impact velocities as

$$\dot{\mathbf{q}}_c^+ = \left(\mathbf{I} - \mathbf{M}_c^{-1}\tilde{\mathbf{W}}_c^T(\tilde{\mathbf{W}}_c\mathbf{M}_c^{-1}\tilde{\mathbf{W}}_c^T)^{-1}\tilde{\mathbf{W}}_c\right)\dot{\mathbf{q}}_c^- = \mathbf{P}_{stick}(\mathbf{q}_c)\dot{\mathbf{q}}_c^- \tag{14}$$

where $\mathbf{I}$ is the $N \times N$ identity matrix. The impact law in (14) can be maintained only if the tangential and normal components of the impulse, denoted by $\tilde{F}_t$ and $\tilde{F}_n$, satisfy the frictional inequality

$$\left|\tilde{F}_t\right| \leq \mu\tilde{F}_n. \tag{15}$$

If the inequality (15) is not satisfied, slippage must occur, so that $\tilde{v}_t(t_c^+) \neq 0$. In that case, it is assumed that the tangential impulse attains its maximal allowed magnitude $\tilde{F}_t = s\mu\tilde{F}_n$, where $s = \pm 1$ is determined by the sign of $\tilde{F}_t$ which is calculated in (13) without considering the friction limitation. In order to compute the normal impulse $\tilde{F}_n$, one has to use the no-rebound requirement $\tilde{v}_n(t_c^+) = 0$ in order to obtain

$$\tilde{\mathbf{w}}_n(\mathbf{q}_c)^T\dot{\mathbf{q}}_c^+ = \tilde{\mathbf{w}}_n(\mathbf{q}_c)^T(\dot{\mathbf{q}}_c^- + \mathbf{M}_c^{-1}\tilde{\mathbf{W}}_c^T\tilde{\mathbf{\Gamma}}\tilde{F}_n) = 0, \text{ where } \tilde{\mathbf{\Gamma}} = \begin{pmatrix} 1 \\ s\mu \end{pmatrix}. \tag{16}$$

From (16), the contact impulse $\tilde{F}_n$ at slipping impact is given by

$$\tilde{\mathbf{F}}_{slip} = \tilde{\mathbf{\Gamma}}\tilde{F}_n = -\tilde{\mathbf{\Gamma}}\left(\tilde{\mathbf{w}}_n(\mathbf{q}_c)^T\mathbf{M}_c^{-1}\tilde{\mathbf{W}}_c^T\tilde{\mathbf{\Gamma}}\right)^{-1}\tilde{\mathbf{w}}_n(\mathbf{q}_c)^T\dot{\mathbf{q}}_c^-. \tag{17}$$

Substituting (17) into (11) then gives a linear relation between the pre-impact and post-impact velocities as

$$\dot{\mathbf{q}}_c^+ = \left(\mathbf{I} - \mathbf{M}_c^{-1}\tilde{\mathbf{W}}_c^T\tilde{\mathbf{\Gamma}}\left(\tilde{\mathbf{w}}_n(\mathbf{q}_c)^T\mathbf{M}_c^{-1}\tilde{\mathbf{W}}_c^T\tilde{\mathbf{\Gamma}}\right)^{-1}\tilde{\mathbf{w}}_n(\mathbf{q}_c)^T\right)\dot{\mathbf{q}}_c^- = \mathbf{P}_{slip}(\mathbf{q}_c)\dot{\mathbf{q}}_c^-. \tag{18}$$

Note that the laws of sticking impact (14) and slipping impact (18) can be combined into a single impact law as $\dot{\mathbf{q}}^+ = \mathbf{P}(\mathbf{q}_c)\dot{\mathbf{q}}^-$, where $\mathbf{P}(\mathbf{q}_c)$ is conditionally defined as $\mathbf{P}_{stick}(\mathbf{q}_c)$ if the inequality (15) is satisfied, and as $\mathbf{P}_{slip}(\mathbf{q}_c)$ otherwise. This impact law is equivalent to Chatterjee's algebraic impact law given in [5] under zero restitution in both normal and tangential directions (i.e. $e = e_t = 0$ in the terminology of [5]). More complicated impact laws can be found in [4, 42, 47]. Usually, the impact is also followed by relabeling of the coordinates in order to account for the switch in the roles of the feet. This is commonly done by applying linear transformations to the positions and velocities $\mathbf{q} \to \mathbf{S}_1\mathbf{q}$ and $\dot{\mathbf{q}} \to \mathbf{S}_2\dot{\mathbf{q}}$ where $\mathbf{S}_1$ and $\mathbf{S}_2$ are constant $N \times N$ matrices.

Note that there exist other possible methods for mathematical formulation of rigid-body dynamics with unilateral frictional contacts, such as complementarity [2, 26, 40] and convex analysis [24, 42] which account for all possible contact interactions in a single equation. Other methods also consider measure-valued contact forces, and thus account for finite forces and impacts in a unified framework [31, 46]. Those methods are beyond the scope of this paper.

2.3. Painlevé's paradox and dynamic jamming. Painlevé's paradox is based on the expression for the contact point normal acceleration, $a_n = \dot{v}_n$, along solutions of (3). Since $v_n = \mathbf{w}_n(\mathbf{q})^T\dot{\mathbf{q}}$, the contact point normal acceleration is given by $a_n = \mathbf{w}_n(\mathbf{q})^T\ddot{\mathbf{q}} + \dot{\mathbf{w}}_n^T\dot{\mathbf{q}}$. Substituting the solution for $\ddot{\mathbf{q}}$ from (3) in the expression for a_n then gives

$$a_n = \mathbf{w}_n^T(q)\mathbf{M}^{-1}(q)\big(-\mathbf{H}(\mathbf{q},\dot{\mathbf{q}}) - \mathbf{G}(\mathbf{q}) + f_n(\mathbf{w}_n(\mathbf{q}) - \sigma\mu\mathbf{w}_t(\mathbf{q}))\big) + \dot{\mathbf{w}}_n^T(\mathbf{q},\dot{\mathbf{q}})\dot{\mathbf{q}}, \tag{19}$$

where $\sigma = \operatorname{sgn}(v_t)$. Collecting the terms of (19) in a compact form gives the key expression ([14, 38]):

$$a_n = -A(\mathbf{q},\dot{\mathbf{q}}) + B(\mathbf{q},\mu)f_n \tag{20}$$

where

$$\begin{aligned} A(\mathbf{q},\dot{\mathbf{q}}) &= \mathbf{w}_n^T(q)\mathbf{M}^{-1}(\mathbf{q})\left(\mathbf{H}(\mathbf{q},\dot{\mathbf{q}}) + \mathbf{G}(\mathbf{q})\right) - \dot{\mathbf{w}}_n^T(\mathbf{q},\dot{\mathbf{q}})\dot{\mathbf{q}} \\ B(\mathbf{q},\mu) &= \mathbf{w}_n^T(\mathbf{q})\mathbf{M}^{-1}(\mathbf{q})\left(\mathbf{w}_n(\mathbf{q}) - \mu\sigma\mathbf{w}_t(\mathbf{q})\right). \end{aligned} \tag{21}$$

Note that B depends on $\dot{\mathbf{q}}$ via the sign variable $\sigma = \mathsf{sgn}(v_t)$. However, the slippage direction and hence σ is constant during any particular time interval of slippage.

Consider the situation where the contact slips with nonzero tangential velocity during a time interval $t \in (-\epsilon, 0)$. During this time interval $a_n = 0$ while $f_n > 0$. If the tangential velocity is non-vanishing at $t = 0$, the instantaneous solution of (20) at this instant can be either continuation of slippage or contact separation. That is, a_n and f_n in (20) must satisfy the linear complementarity relation $0 \le a_n \perp f_n \ge 0$ (cf. [2, 40]). In the case of slippage (20) becomes $0 = -A + Bf_n$. Since $f_n > 0$ during slippage, this dictates that $\mathsf{sgn}(A) = \mathsf{sgn}(B)$ at $t = 0$. In the case of contact separation $f_n = 0$ while $a_n > 0$. In this case (20) becomes $a_n = -A$. Since $a_n > 0$ during contact separation, this dictates that $A < 0$ at $t = 0$. The contact interactions can thus be classified according to the sign of A and B at $t = 0$. The four possible cases are summarized in Table 2.1. Case 1 where $A > 0$ and $B > 0$ corresponds to *consistent slippage.* Case 2 where $A < 0$ and $B > 0$ corresponds to *consistent separation.* Case 3 where $A < 0$ and $B < 0$ is *indeterminate*, as it corresponds to either slippage or separation[1]. Case

[1]Note that a resolution of this indeterminacy was recently proposed in [35] by using the limit of a compliant contact model.

case	sgn(A)	sgn(B)	**solution**	**physical meaning**
1	+	+	$a_n = 0,\ f_n = \frac{A}{B} > 0$	consistent slippage
2	-	+	$f_n = 0,\ a_n = -A > 0$	consistent separation
3	-	-	$f_n = 0,\ a_n = -A > 0$ **or** $a_n = 0,\ f_n = \frac{A}{B} > 0$	indeterminacy
4	+	-	$\emptyset$	inconsistency

TABLE 2.1
Summary of the possible contact interactions during contact slippage.

4 where $A > 0$ and $B < 0$ cannot correspond to slippage since (20) gives $f_n < 0$, nor to contact separation since (20) gives $a_n < 0$. This case is therefore physically inconsistent. Following the terminology in Génot and Brogliato [14], the region in $(\mathbf{q}, \dot{\mathbf{q}})$ space delineated by $A(\mathbf{q}, \dot{\mathbf{q}}) > 0$ and $B(\mathbf{q}, \mu) < 0$ is called the *inconsistency region.*

Dynamic jamming: When a solution approaches the boundary of the inconsistency region it exhibits a peculiar behavior called dynamic jamming, which is defined as follows.

DEFINITION 1. ***Dynamic jamming*** *is a scenario where a solution starts with consistent slippage (case 1) and approaches the inconsistency region (case 4)) with* $B(\mathbf{q}, \mu) \to 0$*, where* f_n *grows unbounded in finite time.*

3. The rimless wheel. This section studies the occurrence of Painlevé's paradox in the dynamics of the rimless wheel (RW) model. The rimless wheel is a star-like body with $n \geq 4$ evenly-spaced spokes (see Figure 3.1(a)), that rolls passively down an inclined plane in a way that resembles bipedal walking. At each time a single spoke is in contact with the ground and represents the stance foot, until the next spoke, which represents the swing foot, hits the ground and makes contact while the previous spoke is released.

We begin by formulating the equations of motion of the RW using the notation introduced in Section 2. Let m and I_c denote the wheel's mass and moment of inertia with respect to its center-of-mass, and let l denote the spokes' length. The gravity acceleration is denoted by g, and the slope angle of the inclined plane is α. The chosen coordinates are $\mathbf{q} = (x, y, \theta)$, where x and y denote the position of the lower spoke's tip in the directions tangent and normal to the ground. Note that this position is constrained, such that $\dot{y} = 0$ means that the wheel maintains contact with the ground, while $\dot{x} = 0$ holds when contact point does not slip. The third coordinate θ is the orientation angle of the lower spoke with respect to the normal direction (y-axis, see Figure 3.1(a)). Thus, θ changes within the range $[-\pi/n, \pi/n]$ between two consecutive "steps", and after an impact at $\theta = \pi/n$ it is reset back to $-\pi/n$ for the next step. Using the unconstrained coordinates $\mathbf{q}$ and velocities $\dot{\mathbf{q}}$, the kinetic and potential energies of the wheel are given by

$$\begin{aligned} \mathcal{T}(\mathbf{q}, \dot{\mathbf{q}}) &= \tfrac{1}{2} m(\dot{x}^2 + \dot{y}^2 + 2\dot{x}\dot{\theta} l \cos\theta + 2\dot{y}\dot{\theta} l \sin\theta) + \tfrac{1}{2}(I_c + ml^2)\dot{\theta}^2 \\ \mathcal{V}(\mathbf{q}) &= mg(y\cos\alpha - x\sin\alpha + l\cos(\alpha + \theta)). \end{aligned} \tag{22}$$

Using the procedure described in Section 2, the continuous-time equations of motion can be derived in the form (3), and the impulse-momentum relation is of the form

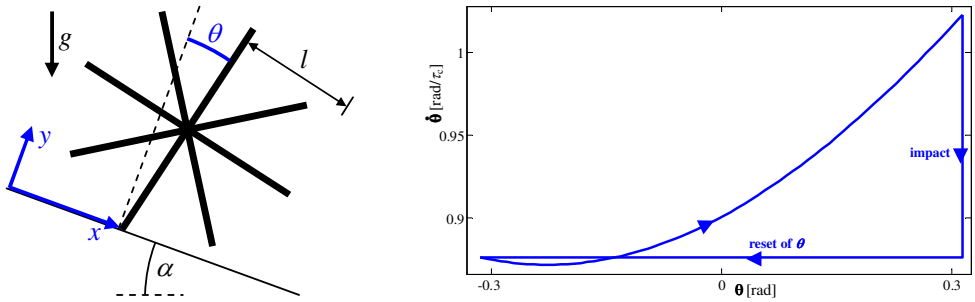

FIG. 3.1. *(a) The rimless wheel (RW) model. (b) Trajectory of periodic solution of the RW in $\theta, \dot{\theta}$-plane under contact sticking.*

(11) where the expressions in these two equations are given as

$$\mathbf{M}(\mathbf{q}) = \begin{pmatrix} m & 0 & ml\cos\theta \\ 0 & m & -ml\sin\theta \\ ml\cos\theta & -ml\sin\theta & ml^2(1+\kappa) \end{pmatrix}, \quad \mathbf{B}(\mathbf{q},\dot{\mathbf{q}}) = \begin{pmatrix} -ml\dot{\theta}^2\sin\theta \\ -ml\dot{\theta}^2\cos\theta \\ 0 \end{pmatrix}, \quad \mathbf{Eu} = \begin{pmatrix} 0 \\ 0 \\ 0 \end{pmatrix}$$
$$\mathbf{G}(\mathbf{q}) = \begin{pmatrix} -mg\sin\alpha \\ mg\cos\alpha \\ -mgl\sin(\alpha+\theta) \end{pmatrix}, \quad \mathbf{W}(\mathbf{q}) = \begin{pmatrix} 1 & 0 & 0 \\ 0 & 1 & 0 \end{pmatrix}, \quad \tilde{\mathbf{W}}_c = \begin{pmatrix} 1 & 0 & 0 \\ 0 & 1 & -2l\sin\frac{\pi}{n} \end{pmatrix} \tag{23}$$

The nondimensional inertia ratio $\kappa{=}I_c/ml^2$ in (23) varies within the range $[0, 1]$, where $\kappa{=}0$ means that all the wheel's mass is concentrated at its center, $\kappa{=}1$ means that all the spokes' masses are concentrated at their tips, and $\kappa{=}1/3$ corresponds to uniform mass distribution along the spokes.

3.1. Review of RW dynamics under sticking contact. We now briefly review known results on the hybrid dynamics of the RW model, which were derived in [7, 28] under the assumption of fully sticking contact . Since the sticking constraint implies that $\dot{x}{=}\dot{y}{=}0$, the equations of continuous-time motion in (3) with the expressions (23) reduce to the single equation for the angle θ:

$$ml^2(1+\kappa)\ddot{\theta} - mgl\sin(\theta+\alpha) = 0. \tag{24}$$

Equation (24) is simply an inverted pendulum equation with a characteristic time of

$$\tau_c = \sqrt{mgl/(ml^2(1+\kappa))}. \tag{25}$$

In the following, time and velocity will be normalized by the characteristic time τ_c. Note that equation (24) is integrable due to conservation of total mechanical energy $\mathcal{T}+\mathcal{V}$, a fact which is exploited in [7, 28] in order to obtain explicit solutions. Impact occurs at $\theta = \pi/n$. Assuming contact sticking, the impact induces a discontinuous jump of the angular velocity $\dot{\theta}$ which can be obtained by (14) as

$$\dot{\theta}^+ = \beta\dot{\theta}^-, \text{ where } \beta = \frac{\cos(2\pi/n)+\kappa}{1+\kappa}. \tag{26}$$

After the impact, the coordinate θ is shifted back from π/n to $-\pi/n$, since the colliding spoke now becomes the new stance foot. In [7, 28], the integrability of (24) is exploited in order to find a periodic solution of the RW system, whose post-impact initial condition is given by

$$\theta(t_c^+) = -\frac{\pi}{n}, \quad \dot{\theta}(t_c^+) = \dot{\theta}^* = 2\beta\sqrt{\frac{\sin\alpha\sin(\pi/n)}{1-\beta^2}}. \tag{27}$$

Moreover, it is shown in [7] that this periodic solution is orbitally stable under small perturbations. This is done by analyzing the linearization of the one-dimensional Poincaré map of this system, which is given explicitly in [7]. As an example, Figure 3.1(b) plots the trajectory of the periodic solution in $\theta, \dot{\theta}$-plane for parameter values of n=10, κ=1/3 and α=13°, where the velocity $\dot{\theta}$ is normalized by the characteristic time τ_c. The vertical line segment corresponds to the jump in $\dot{\theta}$ due to impact, while the horizontal line segment corresponds to re-initialization of θ from π/n back to $-\pi/n$.

In order for the assumption of contact sticking to hold during the entire periodic solution, the contact force $\mathbf{f}$ must satisfy Coulomb's friction constraints (6). Using the expressions (23) and energy conservation of (24), it is shown in [11] that the ratio of tangential-to-normal components of the contact force along the periodic solution of the RW model as a function of θ is given by

$$R(\theta) = \frac{f_t(\theta)}{f_n(\theta)} = \frac{\Big(3\cos(\alpha+\theta) - (\dot{\theta}^*)^2 - 2\cos(\alpha-\pi/n)\Big)\sin\theta - \kappa\sin\alpha}{\Big(3\cos(\alpha+\theta) - (\dot{\theta}^*)^2 - 2\cos(\alpha-\pi/n)\Big)\cos\theta + \kappa\cos\alpha}, \tag{28}$$

where $\dot{\theta}^*$ is given in (27). Thus, the minimal value of friction coefficient required to maintain contact sticking is given by

$$\mu \geq \mu_{stick} = \max\left\{|R(\theta)| : \theta \in \left[-\frac{\pi}{n}, \frac{\pi}{n}\right]\right\}. \tag{29}$$

3.2. Painlevé's paradox in the RW model. We now analyze the occurrence of Painlevé's paradox in the dynamics of the rimless wheel model under contact slippage. This is also relevant in the case of a periodic motion of the RW under contact sticking (i.e. $\dot{x}$=0), which, at some time t_0, is given a kinematic perturbation that enforces slippage $\dot{x}(t_0) \neq 0$. First, we formulate the dynamics of the RW model under contact slippage. The constraint $\dot{x}$=0 no longer holds, and the contact force is determined by (7) and (9). Substituting the expressions in (23) into the equation of motion (3) and the expressions for the contact force in (9), one obtains the equations of motion as

$$\begin{aligned}
\ddot{\theta} &= \frac{\operatorname{sgn}(\dot{x})\,\mu\cos\theta\cdot f_n + m\sin\theta\left(g\cos\alpha - l\cos\theta\cdot\dot{\theta}^2\right)}{ml\left(\sin^2\theta+\kappa\right)} \\
\ddot{x} &= \frac{lm\sin\theta\,(1+\kappa)\,\dot{\theta}^2 - \operatorname{sgn}(\dot{x})\,\mu f_n\,(1+\kappa) + gm\,(\kappa\sin\alpha - \cos(\alpha+\theta)\sin\theta)}{m\left(\sin^2\theta+\kappa\right)}.
\end{aligned} \tag{30}$$

The normal force f_n satisfies equation (20), where the expressions for A and B are given by

$$\begin{aligned}
A(\theta,\dot{\theta}) &= g\cos\alpha - l\dot{\theta}^2\cos\theta \\
B(\theta,\mu) &= \frac{1}{m}\left(\kappa + \sin^2\theta + \sigma\mu\sin\theta\cos\theta\right).
\end{aligned} \tag{31}$$

For a given slippage direction σ=sgn($\dot{x}$), the signs of A and B in (31) depend on θ and $\dot{\theta}$ only, and this, in turn, determines the consistency of slippage according to table

2.1. Painlevé paradox occurs in cases where $B < 0$. Rearranging the expression for B in (31), one obtains

$$B(\theta, \mu) = \frac{1}{2m}\left(1 + 2\kappa - \sqrt{1+\mu^2}\cos(2\theta + \sigma\gamma)\right), \tag{32}$$

where $\gamma = \tan^{-1}(\mu)$ and $\sigma = \pm 1$. The expression for B in (32) can be negative only if the friction coefficient μ is sufficiently large and satisfies

$$\mu > \mu_{min} = 2\sqrt{\kappa + \kappa^2}. \tag{33}$$

Physically, (33) implies that for a given value of μ, the mass of the wheel must be concentrated sufficiently close to its center (lower κ) in order for Painlevé's paradox to occur. For the case where the rimless wheel consists of thin spokes with uniform mass distribution ($\kappa = 1/3$), one obtains $\mu_{min} = 4/3$, which is the same value obtained in [14] for the uniform rod. In case where (33) is satisfied, Painlevé paradox is associated with orientation angles within the range $\theta \in (\theta_1, \theta_2)$, where θ_1 and θ_2 are given by

$$\theta_{1,2} = -\frac{1}{2}\left(\sigma\gamma \mp \arccos\left(\frac{1+2\kappa}{\sqrt{1+\mu^2}}\right)\right). \tag{34}$$

The cases in table 2.1 now define regions in $(\theta, \dot{\theta})$ plane according to the signs of $A(\theta, \dot{\theta})$ and $B(\theta, \mu)$. Figure 3.2(a) plots these regions in $(\theta, \dot{\theta})$ plane for parameter values of κ=0.02, α=10°, n=10, $\mu = 0.35$ and $\sigma = +1$, where region $\mathcal{R}_i$ corresponds to case i in the table for i=1, 2, 3, 4. For these parameter values, the friction coefficient μ is above the minimal value required for occurrence of Painlevé paradox according to (33), which is $\mu_{min} = 0.286$. The orientation angles for which $B(\theta, \mu) < 0$ according to (34) are given by $\theta \in (-0.2644, -0,0723)$ *rad*. On the other hand, the minimal value of μ which is required for existence of a periodic solution of the RW under contact sticking is given by (29) as $\mu_{stick} = 0.32$. Since the chosen value of μ is larger than this lower bound, a periodic solution of the RW under contact sticking exists, and its trajectory in $(\theta, \dot{\theta})$ plane is overlayed on the regions $\mathcal{R}_i$ in Figure 3.2(a). It can be seen that a portion of the periodic solution trajectory under contact sticking intersects the inconsistency region $\mathcal{R}_4$ under forward slippage ($\sigma = +1$). Within this portion of the periodic solution, any small perturbation which involves forward slippage $\dot{x} > 0$ will result in onset of Painlevé's paradox, where no finite-force solution is consistent.

3.3. Dynamic jamming in the RW model. We now demonstrate that the scenario of dynamic jamming can also occur in the RW model, under perturbation of slippage. Dynamic jamming is associated with a solution under initial conditions of consistent slippage, that tends towards the inconsistency region. The conditions for dynamic jamming are thoroughly studied in [14] for the uniform rod, and in [38] for the IPOS mechanism (Figure 1.1(b)). The continuous-time dynamics of the rimless wheel model in (24) is equivalent to a degenerate case of the IPOS model, with $m_1 \to 0$. Thus, the analysis of dynamic jamming in [38] also applies to the RW model, as briefly summarized below.

Dynamic jamming solutions should start at the region $\mathcal{R}_1$ of consistent slippage and evolve towards the inconsistency region $\mathcal{R}_4$. The arrows in Figure 3.2(a) show (qualitatively) the direction of the tangent vector $(\dot{\theta}, \ddot{\theta})$ of solutions in the region $\mathcal{R}_1$. Similar to [38], the directions of these arrows indicate that the only way in which a forward slippage solution can reach the region $\mathcal{R}_4$ is from its left side, i.e. with

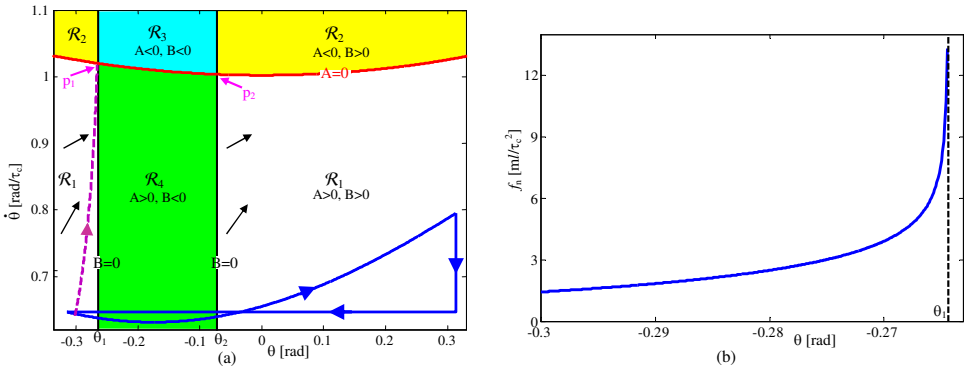

FIG. 3.2. *(a) Regions $\mathcal{R}_i$ of feasibility of cases 1-4 from table 2.1 in $(\theta, \dot{\theta})$ plane. The arrows within $\mathcal{R}_1$ show the direction of tangent vector $(\dot{\theta}, \ddot{\theta})$ under slippage. The closed trajectory is the no-slip periodic solution of the RW under contact sticking. The dashed curve is a solution of dynamic jamming under forward slippage. (b) The normal contact force f_n as a function of θ in the dynamic jamming solution.*

$\theta(0) < \theta_1$. Moreover, it is proven in [14, 38] that such a solution can reach the line $B = 0$ only by converging to the intersection point p_1 at which both $A(\theta, \dot{\theta})$ and $B(\theta, \mu)$ vanish simultaneously. Dynamic jamming is thus obtained when A and B decay to zero in finite time, but $f_n = A/B$ grows unbounded, that is, B decays to zero faster than A. It is also shown in [38] that in order to obtain dynamic jamming, the friction coefficient must be sufficiently large as to satisfy $\mu \geq \mu_c = \frac{2}{\sqrt{3}}\mu_{min}$. In cases where $\mu_{min} < \mu < \mu_c$, the solution crosses the curve A=0 before reaching the line B=0, resulting in f_n=0 and contact separation. Additionally, it is shown in [38] that the initial slippage velocity $\dot{x}(0)$ must be sufficiently large in order to ensure that p_1 is reached before a transition back to contact sticking occurs when the velocity $\dot{x}(t)$ vanishes. As a simulation example, we consider the RW model with the same parameter values of κ=0.02, α=10°, n=10, $\mu = 0.35$, and $l = 1$. The RW is given initial conditions of $\theta(0) = -0.3rad$ and $\dot{\theta}(0) = 0.643rad/\tau_c$ which lie on the periodic solution, but there is an initial slippage velocity of $\dot{x}(0) = 0.5l/\tau_c$. The resulting trajectory in $(\theta, \dot{\theta})$ plane is plotted as the dashed curve in Figure 3.2(a). It can be seen that the trajectory converges to the critical point p_1 at which A=B=0. Figure 3.2(b) plots the normal force f_n as a function of the angle θ. It can be seen that $f_n = A/B$ grows unbounded as $\theta \to \theta_1$. Note that dynamic jamming cannot occur when the initial slippage velocity $\dot{x}(0)$ is arbitrarily small. For the chosen parameter values, dynamic jamming can occur only for $\dot{x}(0) > 0.405$. For lower values of $\dot{x}(0)$, the solution will switch back to contact sticking ($\dot{x} = 0$) before reaching the critical point p_1.

4. The compass biped. This section studies the occurrence of Painlevé's paradox and dynamic jamming in the passive dynamics of the compass biped (CB) model. The compass biped is a robotic model which consists of two rigid links ("legs") of length $2l$, connected by a passive rotary joint ("hip"), see Figure 4.1(a). Each leg has mass m, its center-of-mass lies at the link's center, and the moment of inertia is I_c. Another point mass m_h is located at the hip joint. The robot walks passively on an inclined plane with slope angle α. The angle of the stance leg is $\theta_1(t)$ and the angle of the swing leg is $\theta_2(t)$, both measured with respect to the contact normal (y axis), see Figure 4.1(a). The robot's coordinates are chosen as $\mathbf{q} = (\theta_1, \theta_2, x, y)^T$, where x, y

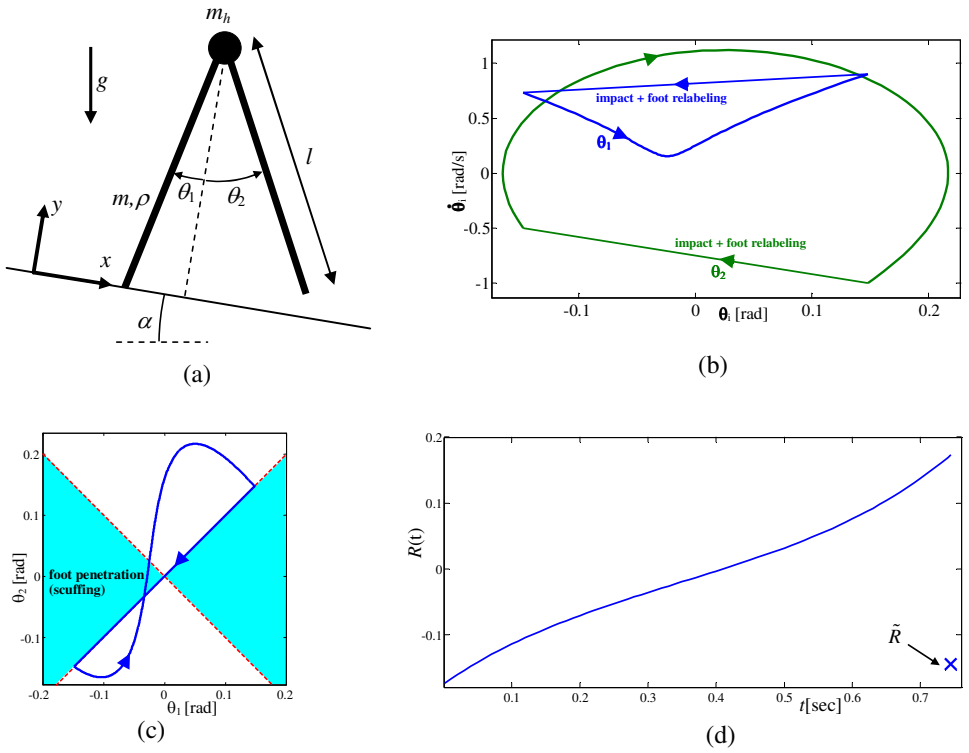

FIG. 4.1. *(a) The compass biped model; Trajectories of a periodic solution under contact sticking in (b) $(\theta_i, \dot{\theta}_i)$-plane, and (c) (θ_1, θ_2)-plane; (d) The force ratio $R(t) = f_t(t)/f_n(t)$ along the periodic solution.*

denote the (constrained) position of the stance foot. Using the formulation procedure described in Section 2, the equations of motion of the robot and impulse-momentum balance can be formulated as in (3) and (11), where the explicit expressions in $\mathbf{q}, \dot{\mathbf{q}}$ are given by

$$\mathbf{M}(\mathbf{q}) = \begin{bmatrix} I_c + (5m+4m_h)l^2 & 2ml^2C_{12} & [3m+2m_h]\,lC_1 & -[3m+2m_h]\,lS_1 \\ 2ml^2C_{12} & I_c+ml^2 & mlC_2 & mlS_2 \\ [3m+2m_h]\,lC_1 & mlC_2 & 2m+m_h & 0 \\ -[3m+2m_h]\,lS_1 & mlS_2 & 0 & 2m+m_h \end{bmatrix}$$

$$\mathbf{H}(\mathbf{q}, \dot{\mathbf{q}}) = \begin{bmatrix} -2ml^2S_{12}\dot{\theta}_2^2 \\ -2ml^2S_{12}\dot{\theta}_1^2 \\ -(3m+2m_h)\,lS_1\dot{\theta}_1^2 - mlS_2\dot{\theta}_2^2 \\ -(3m+2m_h)\,lC_1\dot{\theta}_1^2 + mlC_2\dot{\theta}_2^2 \end{bmatrix} \quad \mathbf{W}(\mathbf{q}) = \begin{bmatrix} 0 & 0 & 1 & 0 \\ 0 & 0 & 0 & 1 \end{bmatrix} \tag{35}$$

$$\mathbf{G}(\mathbf{q}) = g \begin{bmatrix} -(3m+2m_h)\,l\sin(\theta_1+\alpha) \\ -ml\sin(\alpha-\theta_2) \\ -(2m+m_h)\sin\alpha \\ (2m+m_h)\cos\alpha \end{bmatrix} \quad \tilde{\mathbf{W}}(\mathbf{q}) = \begin{bmatrix} 2lC_1 & 2lC_2 & 1 & 0 \\ -2lS_1 & 2lS_2 & 0 & 1 \end{bmatrix} \quad \mathbf{Eu} = \begin{bmatrix} 0 \\ 0 \\ 0 \\ 0 \end{bmatrix}$$

where $S_1 = \sin\theta_1,\ S_2 = \sin\theta_2,\ S_{12} = \sin(\theta_1+\theta_2),\ C_{12} = \cos(\theta_1+\theta_2)$.

The swing foot hits the ground when $\theta_1 = \theta_2$. The impact is then followed by swapping the roles of the swing and stance feet, so that the coordinates of θ_1 and θ_2 and their

velocities are reversed $\theta_i \to -\theta_i,\ \dot{\theta}_i \to -\dot{\theta}_i$.

4.1. Passive dynamics of the CB model under sticking contact. Assuming sticking contact, stable periodic solutions (i.e. gaits) for the passive compass biped have been demonstrated in [28] and extensively studied in [16]. We now show a numerical simulation of a stable periodic solution under sticking contact. The chosen parameter values are l=0.8m, m=4Kg, m_h=2Kg, g=9.8m/s^2, α=1° and I_c=0, (i.e. point masses). The initial conditions of the periodic solution were numerically found as $\theta_1^* = -0.148$, $\dot{\theta}_1^* = 0.733$ and $\dot{\theta}_2^* = -0.501$. Figure 4.1(b) plots the trajectories in $(\theta_i, \dot{\theta}_i)$-plane, where the straight line segments represent the velocity jump at impact and the coordinate relabeling $\theta_i \to -\theta_i,\ \dot{\theta}_i \to -\dot{\theta}_i$. Figure 4.1(c) plots the same periodic trajectory in (θ_1, θ_2) plane. Importantly, the region $\{(\theta_1, \theta_2) :\ |\theta_2| < |\theta_1|\}$ represents infeasible configurations where the swing foot penetrates the ground (shaded regions). However, the resulting periodic solution in Figure 4.1(c) has a portion that passes through this infeasible region. (Only trajectories that pass through the origin θ_1=θ_2=0 can avoid ground penetration). This intermediate penetration, which is called "scuffing", is ignored in our analysis, following the approach of [28] and [16]. Nevertheless, any physical realization of passive bipedal walking must provide a practical solution of foot clearance in order to overcome this foot penetration, as discussed in [28].

Next, we use (5) in order to compute the ratio of tangential-to-normal contact forces at the stance foot. The ratio $R(t) = f_t(t)/f_n(t)$ along the periodic solution is shown in Figure 4.1(d). The plot indicates that the minimal value of friction coefficient required to enforce contact sticking is $\mu_{stick} = 0.175$, which is pretty low for common materials in contact. Moreover, the ratio $\tilde{R}$ of the tangential-to-normal impulse at the impact is marked as '×' at the right end of the plot, and its value is given by $|\tilde{R}|$=0.145 $< \mu_{stick}$. This indicates that as long as $\mu \geq \mu_{stick}$, the contact maintains sticking at the impact as well.

4.2. Painlevé's paradox and dynamic jamming in the CB model. We now study the possible occurrence of Painlevé's paradox and dynamic jamming in the compass biped model under initial slippage. For this model, one cannot easily depict regions $\mathcal{R}_i$ of the different possible cases in table 2.1 as in Figure 3.2(a), since the relevant coordinate-velocity space $(\theta_1, \theta_2, \dot{\theta}_1, \dot{\theta}_2)$ is four-dimensional. The explicit expressions of $A(\mathbf{q}, \dot{\mathbf{q}})$ and $B(\mathbf{q}, \mu)$ are highly complicated, and are given in the Appendix. For a given value of μ and a choice of slippage direction σ, B depends on the angles (θ_1, θ_2) only. Figure 4.2(a) shows the region of $B < 0$ in (θ_1, θ_2) plane for μ=0.7, $\sigma = +1$, while the other parameter values are unchanged. The periodic trajectory under sticking contact is overlayed on the plot, indicating that its initial portion lies within the region of $B < 0$ associated with Painlevé's paradox. It can also be verified numerically that $A(\mathbf{q}, \dot{\mathbf{q}}) > 0$ hold along the entire periodic solution. Therefore, any small initial perturbation of forward slippage in the first part of the periodic solution will lead to case 4 of Painlevé's paradox and solution inconsistency. Figure 4.2(e) demonstrates the dependence of the region $B<0$ on the friction coefficient μ. As μ is decreased, this region shrinks monotonically until it vanishes at the critical value $\mu_{min} \approx 0.5533$. Formulating an explicit expression for μ_{min} as a function of the model parameters is an open problem, which appears to be very challenging due to the complexity of the expressions of A and B. Figure 4.2(f) demonstrates the dependence of the region $B < 0$ on the leg's radius of gyration ρ=$\sqrt{I_c/m}$ for μ=0.8. As ρ is increased, this region shrinks monotonically until it vanishes at the value of

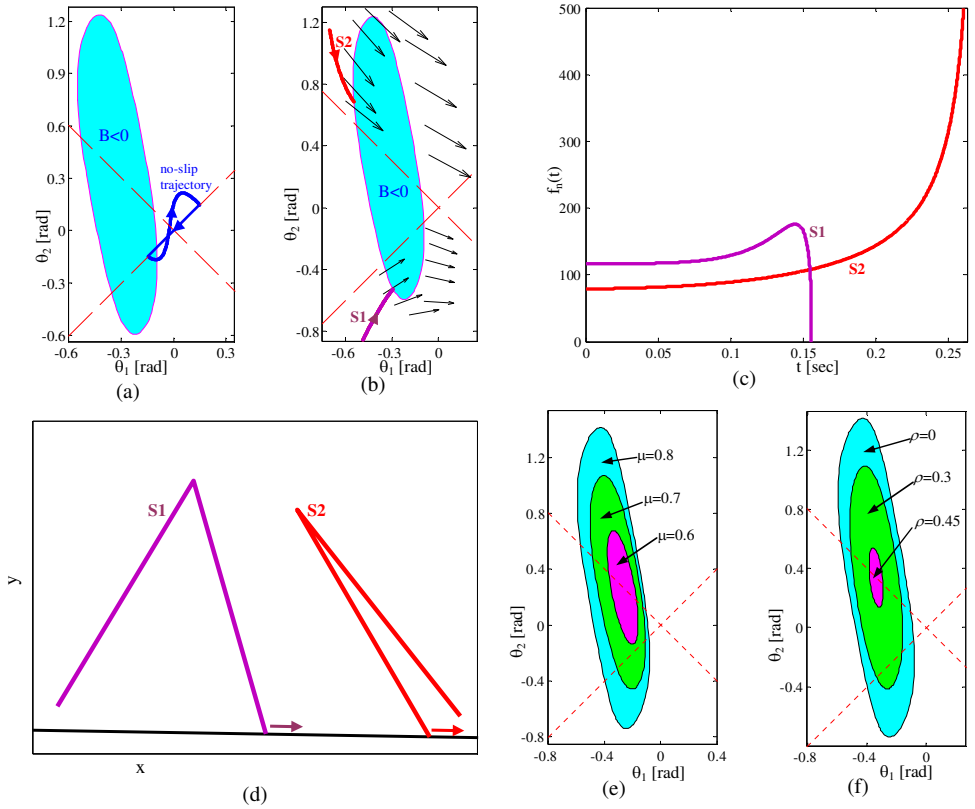

FIG. 4.2. *(a) The region $B < 0$ and the no-slip periodic trajectory in (θ_1, θ_2) plane. (b) Two trajectories S1,S2 of forward slippage that evolve towards the region $B < 0$ in (θ_1, θ_2) plane. The arrows indicate directions of the acceleration vector $(\ddot{\theta}_1, \ddot{\theta}_2)$. (c) The normal contact force $f_n(t)$ along the two trajectories S1,S2. (d) Configurations of the compass biped at the endpoints of the two trajectories S1,S2. (e) The region $B < 0$ for different values of μ. (f) The region $B < 0$ for different values of ρ.*

$\rho \approx 0.4617$.

Next, we demonstrate the occurrence of dynamic jamming in the compass biped model. We were not able to find examples of initial conditions on the no-slip periodic trajectory which are given a perturbation of forward slippage only and result in convergence to the inconsistency region. This is because the acceleration vector $(\ddot{\theta}_1, \ddot{\theta}_2)$ under forward slippage, evaluated on points of the periodic trajectory, always points *away* from the region $B < 0$. Arrows of the direction of the acceleration vector $(\ddot{\theta}_1, \ddot{\theta}_2)$ at some points in (θ_1, θ_2) plane for $\dot{\theta}_1 = \dot{\theta}_2 = 0$ are shown in Figure 4.2(b). It can be seen that only initial conditions on the left side of the inconsistency region are pointing towards it. Thus, these points are suitable candidates of initial conditions that lead to dynamic jamming. As a particular example, the curve marked as S1 in Figure 4.2(b) shows a trajectory of forward slippage under initial angles $\theta_1(0) = -0.2953$, $\theta_2(0) = -0.5247$, while the curve marked as S2 corresponds to initial angles $\theta_1(0) = -0.5461$, $\theta_2(0) = 0.6860$. The other initial conditions for both S1 and S2 are $\dot{\theta}_1(0) = \dot{\theta}_2(0) = 0$ and $\dot{x}(0) = 10$. While both solution trajectories evolve towards the region $B < 0$, solution S1 reaches $A = 0$ first, and thus terminates by contact separation with $f_n = 0$. On the other hand, solution S2 reaches $B = 0$ first so that f_n grows

unbounded. This is precisely the dynamic jamming scenario. Plots of the contact force $f_n(t)$ along both solutions are shown in Figure 4.2(c). This demonstrates that some initial conditions may lead to dynamic jamming while others result in contact separation. The terminal configurations of the compass biped's angles θ_1 and θ_2 in both solutions are shown in Figure 4.2(f).

5. Conclusion. The paper studied the possible occurrence of Painlevé's paradox and dynamic jamming in passive dynamic walking of the rimless wheel and compass biped models. It has been shown that if the periodic solutions under sticking contact are perturbed by a small amount of foot slippage then the solution may suffer from Painlevé paradox, where the only possible solution is tangential impact. Additionally, in the rimless wheel model a finite-size perturbation of slippage close to the no-slip periodic solution may lead to dynamic jamming where the solution approaches an inconsistent configuration and the contact force grows unbounded. In the compass biped model, dynamic jamming was obtained only for initial conditions of finite slippage that lie far from the periodic solution. Two key parameters were identified that critically influence the likelihood of occurrence of Painlevé's paradox and dynamic jamming: large coefficient of friction and small radius of gyration, i.e. most of the mass is concentrated close to body's center. The results indicate that the phenomena of Painlevé's paradox and dynamic jamming are of crucial importance for robotic legged locomotion, and that initial perturbations that involve foot slippage may cause undesired and unpredictable outcomes.

Next, limitations of the results in this paper are briefly discussed, and possible directions of future research are proposed. First, the results clearly indicate that there is a need for a new definition of orbital stability in mechanical systems with unilateral contacts, that accounts for position-and-velocity perturbations that involve all possible contact interactions. That is, stability (stabilization) of a periodic no-slip solution of a passive (actuated) dynamically walking robot should be assessed also with respect to perturbations that involve contact separation or slippage. Some attempts to define and analyze this type of stability for frictional equilibrium postures or equilibrium sets were conducted in [24, 37, 50]. Nevertheless, a complete characterization and generalization of this notion to orbital stability of periodic solutions is currently an open problem. Second, the paper only shows *in theory* that Painlevé's paradox and dynamic jamming are relevant to legged robotic systems. Experimental demonstration these phenomena in practical situations has not yet been done, and remains as a challenging future task, which might prove to be very difficult, if not impossible.

As for further generalizations of the theoretical study of Painlevé's paradox and dynamic jamming, it is proposed to extend the analysis to the case of curved contact surfaces, rather than (vertex-edge) point contacts [14, 27, 39] or (edge-edge) flat contacts [38]. Inspired by preliminary analysis proposed in [13], incomplete investigation by the author (unpublished) indicates that adding contact curvature has a strong influence on the likelihood of occurrence of Painlevé's paradox even for practical values of friction and mass distribution. Additionally, the analysis of conditions for dynamic jamming based on the behavior of solutions in the vicinity of the critical points p_i at which $A{=}B{=}0$ was limited to the rod [14] and IPOS [38] models, where the dynamics evolve in the two-dimensional state space of a single coordinate, namely $(\theta, \dot{\theta})$. Even the simple case of the compass biped where the dynamics evolve in the state space of $(\theta_1, \theta_2, \dot{\theta}_1, \dot{\theta}_2)$ was only investigated numerically in this work. Generalization of the results in [14, 38] to an n degrees-of-freedom (DOF) system (yet with a single contact)

should be complicated, since the critical point defined by $A{=}B{=}0$ now becomes a hypersurface of dimension $2n-2$ (e.g. dimension 2 in the compass biped model) which can be reached only at some regions depending on the direction of acceleration $\ddot{\mathbf{q}}$, as hinted in the numerical analysis of Section 4. In fact, even generalizing the explicit expressions analogous to μ_{min} and μ_c (minimal value of μ required for occurrence of Painlevé's paradox and dynamic jamming, respectively) to the case of n DOF is currently an open problem. Finally, Painlevé's paradox can also occur in systems with *multiple* frictional contacts, as shown in preliminary analysis in [36] of a single rigid body with two slipping contacts. A complete theory of Painlevé's paradox for the general case of n DOF and k contacts has not yet been explored.

Appendix - Expressions of A and B for the compass biped model. The expressions for $A(\mathbf{q},\dot{\mathbf{q}})$ and $B(\mathbf{q},\mu)$ from Eq. (21) for the compass biped under forward slippage $\boldsymbol{\sigma}{=}+1$ are given by

$$A(\mathbf{q},\dot{\mathbf{q}}) = \frac{N_A(\theta_1,\theta_2,\dot{\theta}_1,\dot{\theta}_2)}{2\Delta(\theta_1,\theta_2)} \text{ and } B(\mathbf{q},\mu) = \frac{N_B(\theta_1,\theta_2,\mu)}{\Delta(\theta_1,\theta_2)} \text{ , where}$$

$$\begin{aligned}
N_A(\theta_1,\theta_2,\dot{\theta}_1,\dot{\theta}_2) = {}& -2l(8I_c^2m_h^2C_1+24I_c^2m^2C_1+28I_c^2mm_hC_1+8l^4m^2m_h^2C_1\\
&+52l^2m^2I_cm_hC_1+46l^2m^3I_cC_1+16l^2mI_cm_h^2C_1+14l^4m^4C_1-12l^2m^2I_cm_h\cos(\theta_1+2\theta_2)\\
&-18l^4m^3m_h\cos(\theta_1+2\theta_2)-22l^2m^3I_c\cos(\theta_1+2\theta_2)+6l^4m^3m_h\cos(3\theta_1+2\theta_2)\\
&-29l^4m^4\cos(\theta_1+2\theta_2)+15l^4m^4\cos(3\theta_1+2\theta_2)+24l^4m^3m_hC_1)\dot{\theta}_1^2\\
&+2lm(-3m^3l^4\cos(2\theta_1+3\theta_2)-14m^3l^4C_2+17m^3l^4\cos(2\theta_1+\theta_2)-22m^2l^2I_cC_2\\
&-18m^2l^4m_hC_2+30m^2l^2I_c\cos(2\theta_1+\theta_2)+22m^2l^4m_h\cos(2\theta_1+\theta_2)-6ml^4m_h^2C_2+8mI_c^2C_2\\
&-20ml^2I_cm_hC_2+6ml^4m_h^2\cos(2\theta_1+\theta_2)+28ml^2I_cm_h\cos(2\theta_1+\theta_2)-6l^2m_h^2I_cC_2\\
&+4I_c^2m_hC_2+6l^2m_h^2I_c\cos(2\theta_1+\theta_2))\dot{\theta}_2^2+(8m^3l^4m_hC_\alpha+8ml^2I_cm_h^2C_\alpha+4m^2l^4m_h^2C_\alpha\\
&+16I_c^2mm_hC_\alpha+16I_cC_\alpha l^2m^3+2C_\alpha l^4m^4+16I_c^2C_\alpha m^2+4I_c^2m_h^2C_\alpha\\
&+24m^2l^2I_cm_hC_\alpha-l^4m^4\cos(-2\theta_1-2\theta_2+\alpha)-l^4m^4\cos(2\theta_1+2\theta_2+\alpha))g
\end{aligned}$$

$$\begin{aligned}
N_B(\theta_1,\theta_2,\mu) = {}& -l^4(-7+2\cos(2\theta_2)-\cos(2\theta_1+2\theta_2)+6\cos(2\theta_1)+2\sin(2\theta_2)\mu\\
&-6\sin(2\theta_1)\mu)m^3+(-l^4(-7+5\cos(2\theta_1)-5\sin(2\theta_1)\mu)m_h-l^2I_c(-9\sin(2\theta_1)\mu+\sin(2\theta_2)\mu\\
&+\cos(2\theta_2)-14+9\cos(2\theta_1)))m^2+(-l^4(\cos(2\theta_1)-\sin(2\theta_1)\mu-1)m_h^2-2l^2I_c(-3\sin(2\theta_1)\mu\\
&-5+3\cos(2\theta_1))m_h+4I_c^2)m-l^2I_c(\cos(2\theta_1)-\sin(2\theta_1)\mu-1)m_h^2+2I_c^2m_h
\end{aligned}$$

$$\begin{aligned}
\Delta(\theta_1,\theta_2) = {}& -l^4(-1+\cos(2\theta_1+2\theta_2))m^4+(8l^2I_c+4l^4m_h)m^3\\
&+(12l^2I_cm_h+8I_c^2+2m_h^2l^4)m^2+(4m_h^2l^2I_c+8I_c^2m_h)m+2I_c^2m_h^2
\end{aligned}$$

$C_1=\cos(\theta_1),\ C_2=\cos(\theta_2),\ C_\alpha=\cos(\alpha).$

REFERENCES

[1] A. D. Ames, K. Galloway, J. W. Grizzle, and K. Sreenath, *Rapidly exponentially stabilizing control Lyapunov functions and hybrid zero dynamics*, IEEE Transactions on Automatic Control, (to appear).

[2] M. Anitescu and F. A. Potra, *Formulating dynamic multi-rigid-body contact problems with friction as solvable linear complementarity problems*, Nonlinear Dynamics, 14 (1997), pp. 231–247.

[3] M. D. Berkemeier and R. S. Fearing, *Sliding and hopping gaits for the underactuated acrobot*, IEEE Trans. Robotics and Automation, 14 (1998), pp. 629–634.

[4] B. Brogliato, *Nonsmooth Mechanics*, Springer-Verlag, 1999.

[5] A. Chatterjee and A. Ruina, *A new algebraic rigid body collision law based on impulse space considerations*, ASME Journal of Applied Mechanics, 65 (1998), pp. 939–951.

[6] M. J. Coleman, A. Chatterjee, and A. Ruina, *Motions of a rimless spoked wheel: A simple 3D system with impacts*, Dynamics and Stability of Systems, 12 (1997), pp. 139–160.

[7] M. J. Coleman and A. Ruina, *Dynamics and stability of a rimless spoked wheel: a simple 2D system with impacts*, Dynamical Systems: an International Journal, 25 (2010), pp. 215–238.

[8] S. Collins, A. Ruina, R. Tedrake, and M. Wisse, *Efficient bipedal robots based on passive dynamic walkers*, Science, 307 (2005), pp. 1082–1085.

[9] S. H. Collins, M. Wisse, and A. Ruina, *A 3-D passive dynamic walking robot with two legs and knees*, International Journal of Robotics Research, 20 (2001), pp. 607–615.

[10] P. E. Dupont and S. P. Yamajako, *Jamming and wedging in constrained rigid-body dynamics*, in IEEE Int. Conf. on Robotics and Automation, 1994, pp. 2349–2354.

[11] B. Gamus and Y. Or, *Analysis of dynamic bipedal robot locomotion with stick-slip transitions*, in Proceedings of IEEE International Conference on Robotics and Automation, 2013, pp. 3333–3340.

[12] ———, *Analysis of dynamic bipedal robot locomotion with stick-slip transitions*, (to be submitted).

[13] F. Génot, *Contributions a la modelisation et a la commande des systemes mecaniques de corps rigides avec contraintes unilaterales*, PhD thesis, Polytechnique de Grenoble, 1998.

[14] F. Génot and B. Brogliato, *New results on Painlevé paradoxes.*, European J. of Mechanics– A/Solids, 18 (1999), pp. 653–677.

[15] R. Goebel, R. G. Sanfelice, and A. R. Teel, *Hybrid dynamical systems*, IEEE Control Systems Magazine, 29 (2009), pp. 28–93.

[16] A. T. Goswami, *A study of the passive gait of a compass-like biped robot: Symmetry and chaos*, International Journal of Robotics Research, 17 (1998), pp. 1282–1301.

[17] J. W. Grizzle, C. Chevallereau, A. D. Ames, and R. Sinnet, *3D bipedal robotic walking: Models, feedback control, and open problems*, in Proc. 8th IFAC Symposium on Nonlinear Control Systems (NOLCOS), 2010, pp. 505–532.

[18] J. Guckenheimer and P. Holmes, *Nonlinear Oscillations, Dynamical Systems, and Bifurcations of Vector Fields*, Springer-Verlag, New York, 1983.

[19] B. Hall and A. Champneys, *Why does chalk squeak?*, technical report, Dept. of Eng. Math., University of Bristol, 2009, in `www.enm.bris.ac.uk/teaching/projects/2008_09/bh5217/download/Chalk_Report.pdf`.

[20] Y. Hurmuzlu, F. Génot, and B. Brogliato, *Modeling, stability and control of biped robots—a general framework*, Automatica, 40 (2004), pp. 1647–1664.

[21] P. R. Kraus, V. Kumar, and P. Dupont, *Analysis of frictional contact models for dynamic simulation*, in IEEE Int. Conf. on Robotics and Automation, 1998, pp. 2822–2827.

[22] A. D. Kuo, *Stabilization of lateral motion in passive dynamic walking*, International Journal of Robotics Research, 18 (1999), pp. 917–930.

[23] R. I. Leine, B. Brogliato, and H. Nijmeijer, *Periodic motion and bifurcations induced by the Painlevé paradox.*, European Journal of Mechanics– A/Solids, 21 (2002), pp. 869–896.

[24] R. I. Leine and N. van de Wouw, *Stability properties of equilibrium sets of nonlinear mechanical systems with dry friction and impact*, Nonlinear Dynamics, 51 (2008), pp. 551–583.

[25] C. Liu, Z. Zhao, and B. Chen, *The bouncing motion appearing in a robotic system with unilateral constraint*, Nonlinear Dynamics, 49 (2007), pp. 217–232.

[26] P. Lotstedt, *Coulomb friction in two-dimensional rigid body systems*, Zeitschrift fur Angewandte Mathematik und Mechanik, 61 (1981), pp. 605–615.

[27] M. T. Mason and Y. Wang, *On the inconsistency of rigid-body frictional planar mechanics*, in IEEE Int. Conf. on Robotics and Automation, 1988, pp. 524–528.

[28] T. McGeer, *Passive dynamic walking*, International Journal of Robotics Research, 9 (1990), pp. 62–82.

[29] ———, *Passive walking with knees*, in Proceedings of IEEE International Conference on Robotics and Automation, vol. 3, 1990, pp. 1640 – 1645.
[30] D. Meltz, Y. Or, and E. Rimon, *Experimental verification and graphical characterization of dynamic jamming in frictional rigid-body mechanics*, in IEEE Int. Conf. on Robotics and Automation, 2007, pp. 580–585.
[31] J. J. Moreau, *Unilateral contact and dry friction in finite freedom dynamics*, in Nonsmooth Mechanics and Applications, vol. 302 of CISM Courses and lectures, Springer-Verlag, 1988, pp. 1–82.
[32] B. Morris and J. W. Grizzle, *Hybrid invariant manifolds in systems with impulse effects with application to periodic locomotion in bipedal robots*, IEEE Transactions on Automatic Control, 54 (2009), pp. 1751–1764.
[33] M. P. Murphy, A. Saunders, C. Moreira, A. A. Rizzi, and M. Raibert, *The LittleDog robot*, International Journal of Robotics Research, 30 (2011), pp. 145–149.
[34] R. M. Murray, Z. Li, and S. Sastry, *A Mathematical Introduction to Robotic Manipulation*, CRC Press, 1993.
[35] A. Nordmark, H. Dankowicz, and A. Champneys, *Friction-induced reverse chatter in rigid-body mechanisms with impacts*, IMA Journal of Applied Mathematics, 76 (2011), pp. 85–119.
[36] Y. Or, *Frictional Equilibrium Postures for Robotic Locomotion - Computation, Geometric Characterization, and Stability Analysis*, PhD thesis, Technion, Haifa, Israel, 2007.
[37] Y. Or and E. Rimon, *On the hybrid dynamics of planar mechanisms supported by frictional contacts. I: Necessary conditions for stability*, in IEEE Int. Conf. on Robotics and Automation, 2008, pp. 1213 – 1218.
[38] ———, *Investigation of Painlevé's paradox and dynamic jamming during mechanism sliding motion*, Nonlinear Dynamics, 67 (2012), pp. 1647–1668.
[39] P. Painlevé, *Sur les lois du frottement de glissement*, Comptes Rendus De L'Acadamie Des Sciences, (1895), pp. 112–115.
[40] J.S. Pang and J.C. Trinkle, *Complementarity formulations and existence of solutions of dynamic multi-rigid-body contact problems with Coulomb friction*, Mathematical Programming, 74 (1996), pp. 199–226.
[41] J.-S. Pang, *Frictional contact models with local compliance: Semismooth formulation*, Zeitschrift fur Angewandte Mathematik und Mechanik, 88 (2008), pp. 454–471.
[42] F. Pfeiffer and C. Glocker, *Multibody Dynamics with Unilateral Contacts*, John Wiley & Sons, New York, 1996.
[43] M. Raibert, K. Blankespoor, G. Nelson, R. Playter, and the Bigdog Team, *BigDog, the rough-terrain quadruped robot*, in Proceeding of the 17th IFAC World Congress, 2008, pp. 10822–10825.
[44] P. Song, J.-S. Pang, and V. Kumar, *A semi-implicit time-stepping model for frictional compliant contact problems*, International Journal for Numerical Methods in Engineering, 60 (2004), pp. 2231–2261.
[45] D.E. Stewart, *Convergence of a time-stepping scheme for rigid body dynamics and resolution of Painlevé's problem*, Archive for Rational Mechanics and Analysis, 145 (1998), pp. 215–260.
[46] D. E. Stewart and J. C. Trinkle, *An implicit time-stepping scheme for rigid body dynamics with inelastic collisions and Coulomb friction*, Int. J. of Numerical Methods in Engineering, 39 (1996), pp. 2673–2691.
[47] W. J. Stronge, *Impact Mechanics*, Cambridge University Press, Cambridge, UK, 1979.
[48] A. Tavakoli and Y. Hurmuzlu, *Robotic locomotion of three generations of a family tree of dynamical systems, part I: Passive gait patterns*, Nonlinear Dynamics, 73 (2013), pp. 1969–1989.
[49] R. Tedrake, T. W. Zhang, M. Fong, and H. S. Seung, *Actuating a simple 3D passive dynamic walker*, in Proceedings of IEEE International Conference on Robotics and Automation, 2003, pp. 4656–4661.
[50] P. L. Varkonyi, D. Gontier, and J. W. Burdick, *On the Lyapunov stability of quasistatic planar biped robots*, in Proceedings of IEEE International Conference on Robotics and Automation, 2012, pp. 63–70.
[51] J. A. Vazquez and M. Velasco-Villa, *Numerical analysis of the sliding effects of a 5-dof biped robot*, in 8th International Conference on Electrical Engineering Computing Science and Automatic Control, 2011, pp. 1–6.
[52] Y. Wang and M. T. Mason, *Two-dimensional rigid body collisions with friction*, J. of Applied Mechanics, 10 (1993), pp. 292–352.
[53] E. R. Westervelt, J. W. Grizzle, C. Chevallereau, J. H. Choi, and B. Morris, *Feedback*

Control of Dynamic Bipedal Robot Locomotion, CRC Press, 2007.
[54] M. Wisse, *Three additions to passive dynamic walking: Actuation, an upper body, and 3D stability*, International Journal of Humanoid Robotics, 2 (2005), pp. 459–478.
[55] Z. Zhao, C. Liu, W. Ma, and B. Chen, *Experimental investigation of the Painlevé paradox in a robotic system*, Journal of Applied Mechanics, 75 (2007), p. 041006.